Available online at www.sciencedirect.com
ScienceDirect
Biosensors and Bioelectronics 23 (2008) 1003–1009
BIOSENSORS & BIOELECTRONICS
www.elsevier.com/locate/bios

Label-free quantitative DNA detection using the liquid core optical ring resonator

Jonathan D. Suter [a], Ian M. White [a], Hongying Zhu [a], Huidong Shi [b], Charles W. Caldwell [b], Xudong Fan [a,*]

[a] *Department of Biological Engineering, 240D Bond Life Sciences Center, University of Missouri-Columbia, Columbia, MO 65211, United States*
[b] *Department of Pathology and Anatomical Sciences, University of Missouri-Columbia, Columbia, MO 65211, United States*

Received 30 June 2007; received in revised form 31 August 2007; accepted 12 October 2007
Available online 22 October 2007

Abstract

We demonstrated quantitative real-time label-free detection of DNA sequences using the liquid core optical ring resonator (LCORR) sensor. The LCORR is a recently developed sensing platform that integrates microfluidics and photonic sensing technology with low detection limit and sub-nanoliter detection volume. We analyzed experimentally and theoretically the LCORR response to a variety of DNA samples that had different strand lengths (25–100 bases), number of base- mismatches (1–5), and concentrations (10 pM to 10 μM) to evaluate the LCORR sequence detection capability. In particular, we established the linear correlation between the LCORR sensing signal and the molecule density, which allows us to accurately calculate the molecule density on the surface. It is found that the probe surface coverage was 26–51% and the extent of hybridization was 40–50%. The titration curve for 25-base probe and 25-base target DNA yields a dissociation constant of 2.9 nM. With a 37.1 nm/RIU LCORR, detection of 10 pM bulk DNA concentration was demonstrated. The mass detection limit was estimated to be 4 pg/mm^2, corresponding to a density of 10^{10} molecules/cm^2 on the surface. We also showed that the LCORR was sensitive enough to differentiate DNA with only a few base-mismatches based on the raw sensing signal and kinetic analysis. Our work will provide important insight into the light-DNA interaction at the ring resonator surface and lay a foundation for future LCORR-based DNA label-free microarray development.

Keywords: DNA detection; Refractometric detection; Label-free; Optical ring resonator; Microfluidics

1. Introduction

Highly specific DNA detection is very important in many applications including medicine, food safety, and forensic studies (Gill et al., 1985; Luong et al., 1997; Christopoulos, 1999; Fortina et al., 2002). Currently, the most popular method is fluorescent microarray technology (Guo et al., 1994; Charles et al., 2003). However, quantitative analysis of DNA has been challenging due to the fluorescence signal bias, as the number of fluorophores on each DNA target molecule cannot be precisely controlled (Cox and Singer, 2004). Furthermore, microarrays do not offer real-time signal acquisition, and thus kinetic information that can be used to reduce the false positives is lost. Optical label-free detection of analytes in their native forms has been under intensive investigation to address the limitations in microarrays (Lin et al., 2002; Ramachandran et al., 2005). Most label-free systems also allow real-time data collection for kinetic analysis. A notable type of label-free sensor is the surface plasmon resonance (SPR) sensor (Homola et al., 1999; Chinowsky et al., 2003), which is exemplified by the instruments commercialized by both Biacore and Spreeta.

Label-free detection can also be achieved by optical waveguides (Passaro et al., 2007) or optical fibers (Golden et al., 1994). In these systems, an evanescent field extends beyond the surface of the waveguide or fiber cable; analytes deposited onto the waveguide surface are in the path of the evanescent field, and thus they change the effective refractive index (RI) experienced by the guided mode. Since the sensing signal is accumulative

* Corresponding author. Tel.: +1 573 884 2543; fax: +1 573 884 9676.
E-mail address: fanxud@missouri.edu (X. Fan).

0956-5663/$ – see front matter © 2007 Elsevier B.V. All rights reserved.
doi:10.1016/j.bios.2007.10.005

along the waveguide, they must be as much as a few centimeters in length in order to achieve larger signals and low detection limits (Schneider et al., 2000; Passaro et al., 2007; Araci et al., 2007).

Optical microring resonators are a special type of a waveguide in which the light circulates along the ring-shaped waveguide numerous times in the form of the whispering gallery modes (WGM) (Gorodetsky and Ilchenko, 1999), thus significantly increasing the interaction length between the light and the analyte. The effective light–analyte interaction length, L_{eff}, is governed by $L_{\text{eff}} = Q\lambda/2\pi n$ (Gorodetsky et al., 1996), where Q is the ring resonator Q-factor, λ is the WGM resonant wavelength, and n is the RI of the ring resonator. For a Q-factor of 10^6, L_{eff} can be 16 cm at $\lambda = 1550$ nm, although the typical size of a ring is only 10–300 μm in diameter. Recently, very sensitive planar waveguide-based (Chao et al., 2006; Passaro et al., 2007) and stand-alone microsphere-based (Vollmer et al., 2002, 2003) ring resonator biosensors have been demonstrated. In fact, a detection limit of 6 pg/mm^2 for hybridization-based DNA detection has been achieved using microsphere ring resonators (Vollmer et al., 2003).

While microsphere-based sensors exhibit high Q-factor (>10^6 in water) (Vollmer et al., 2002, 2003) and low detection limit, fluidic integration, mass production, and reproducibility are extremely difficult. On the other hand, planar ring resonators can be mass-produced relatively easily through lithographic or imprint technologies, but they suffer from relatively low Q-factor (10^4 in water) (Chao et al., 2006; Passaro et al., 2007). Furthermore, incorporation of fluidics is very challenging, as the fluidics needs to be fabricated separately and then mounted onto ring resonator sensors through multiple steps.

The liquid core optical ring resonator (LCORR) (White et al., 2006a) is a novel opto-fluidic device that integrates ring resonator sensing technology into the microfluidics. Fig. 1(A) displays a schematic of the LCORR sensing mechanism. Fig. 1(B) displays the entire LCORR mounted in its experimental setup. The LCORR utilizes a glass capillary as a microfluidic channel and its circular cross-section forms the ring resonator that supports the WGM. The capillary wall is sufficiently thin (2–4 μm) so that the evanescent field of the WGM is present in the core and interacts with the analyte near the LCORR interior surface when the sample is passed through the capillary (White et al., 2006a). This internal surface sensing is a unique feature that enables advanced photonic integration because the fluid is conducted through the inside of the capillary while the optical interface is on the outer surface, as shown later.

The LCORR performs the label-free detection by monitoring the WGM resonant wavelength, λ, which is given by (Gorodetsky and Ilchenko, 1999):

$$2\pi n_{\text{eff}} r = m\lambda, \tag{1}$$

where n_{eff} is the effective RI of the media encountered by the WGMs, r is the capillary radius, and m is an integer multiple representing the mode's angular momentum term. n_{eff} is determined by the RI of the core, the wall, and the surrounding medium. When biomolecules attach to the LCORR interior surface, the RI near the LCORR surface changes, and thus the WGM resonant wavelength changes. Therefore, the temporal response of the WGM spectral position conveys the quantitative and kinetic information regarding the biomolecule binding to the LCORR surface.

The LCORR takes advantage of the superior fluidic handling capability of a capillary and the excellent detection capability of the ring resonator. Additionally, since each ring along a capillary can be as short as a few tens of microns (Fan et al., 2007), sub-nL detection volume per ring resonator can be achieved. It also benefits from reduced diffusion times due to small dimensions and large surface-to-volume ratio resulting from the circular fluidic channel. Furthermore, the LCORR can potentially be scaled up into a two-dimensional array for multiplexed detection. It is estimated that thousands of ring resonator sensors can be packed onto a 1 cm^2 chip. This sort of array will provide a promising and complementary technology to traditional fluorescence-based DNA microarrays.

In this paper, we used a single LCORR as a model system to develop the protocol for LCORR DNA hybridization assays. Furthermore, the LCORR response (WGM spectral shift) to various DNA samples was experimentally and theoretically analyzed in order to evaluate DNA detection capability of the LCORR. We know that the LCORR is able to detect DNA concentrations down to 10 pM. It has also been estimated that we can detect as little as 4 pg/mm^2 mass density on the LCORR surface. Compared to other label-free technologies this perfor-

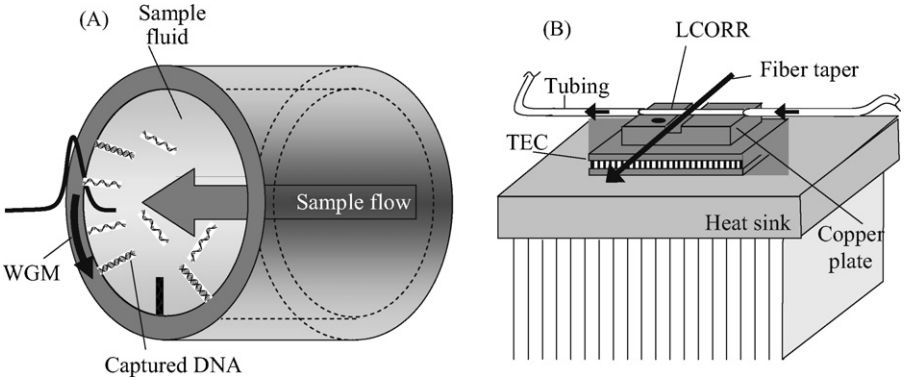

Fig. 1. (A) Cross-sectional diagram of an individual LCORR sensor. (B) Side view of the experimental setup.

mance is quite comparable. DNA studies with localized SPR on gold nanoparticles have demonstrated best limits of detection (LOD's) of 10 pM and ~100 fg/mm^2 (Lin et al., 2000). Evanescent waveguides have yielded LOD's of 300 pM (Sepulveda et al., 2006) and protein surface densities as good as 20 fg/mm^2 (Ymeti et al., 2007). Base-mismatched DNA hybridization was also investigated through the net spectral shift and kinetic response of the WGM. Our results will provide insight into the interaction between biomolecules (specifically DNA) and the WGM and will lay a solid foundation for future label-free DNA microarray development.

2. Experimental methods

2.1. Materials

Reagents used in this study included 98% ethanol, 12 M HCl, anhydrous methanol, 48% hydrofluoric acid (HF), and 3-aminopropyltrimethoxysilane (3-APS), all obtained from Sigma–Aldrich. 3× SSC running buffer was produced in-house using 0.45 M NaCl and 0.045 M sodium citrate in purified water. Homobifunctional amine-reactive crosslinking agent dimethyl adipimidate (DMA) was obtained from Aldrich. 18 MΩ water purified by an Easypure-UV system from Barnstead was used in all solutions. Glass capillaries were purchased from Sutter Instruments. All DNA samples used in the experiments were custom strands made by Sigma Genosys and were designed specifically to reduce the probability of secondary structure formation using online mfold software (Rensselaer Polytechnic Institute) (Zuker, 2003). The aminated probe strands designed in this manner had the sequence, 5′-NH_2-C_6-CCA ACC AGA GAA CCG CAG TCA CAA T-3′.

For the purpose of mismatch discrimination the target sequence was modified in the following way, with bolded letters indicating mismatched nucleotides:

- 1-base mismatch: 5′-ATT GTG ACT GCG **C**TT CTC TGG TTG G-3′
- 2-base mismatch:5′-ATT GTG ACT **C**CG **C**TT CTC TGG TTG G-3′
- 5-base mismatch: 5′-ATT GTG ACT **CG**G **CAA** CTC TGG TTG G-3′

For experiments using longer targets, a 50-mer was ordered with a sequence of 5′-ATT GTG ACT GCG GTT CTC TGG TTG GAC TTG TGA CTG GCT TCT ATG GTT GG-3′ and a 100-mer was ordered with a sequence of 5′- ATT GTG ACT GCG GTT CTC TGG TTG GAC TTG TGA CTG GCT TCT ATG GTT GGA TTG TGA CTT CGG TTC TCT GGT TGG ACT TGT GAC TGG CTT CTA TGG TTG G-3′. The first 25 bases are identical in all three strand lengths so that the same probe length and sequence may be used for each experiment.

2.2. Experimental setup

An LCORR of 100 μm in outer diameter (OD) was fabricated by pulling a quartz capillary under intense heat (~2000 °C) followed by HF etching from inside, as has been detailed in previous work (White et al., 2006a; Fan et al., 2007). Then the LCORR's and optical fibers were mounted orthogonally on the sensor platform as shown in Fig. 1(B). The LCORR was fixed onto a copper plate (1 cm^2) that, in turn, sat on top of a thermo-electric cooler (TEC) unit (Marlow Industries, Inc.) connected to a temperature controller (ILX Lightwave). A thermister was embedded in the copper plate near the coupling region with thermally conductive epoxy (Arctic Silver). A custom fitted acrylic cap was placed on top of the copper plate to protect the system from air current disruption. Fluidic delivery was handled by a syringe pump (Harvard Apparatus) and Tygon tubing. All experiments were performed at room temperature (~25 °C).

The WGM was launched inside the circumference of the LCORR with the 1550 nm tunable diode laser (JDS Uniphase) scanned across a range of 100 pm at a scanning rate of 2 Hz. Light was guided to the LCORR with a single-mode optical fiber that was tapered to approximately 3 μm in diameter at the coupling location. At its output, the fiber was directed at a photodetector to collect a spectral intensity dataset. When the laser wavelength is on resonance with the WGM, a spectral dip was observed at the fiber output, indicating the WGM spectral position (Zhu et al., 2007b). The Q-factor for the WGM, which was deduced from the full-width at the half maximum of the resonance dip, was approximately 10^6 (White et al., 2007).

2.3. LCORR bulk refractive index sensitivity (BRIS) characterization

Prior to DNA detection, the BRIS was measured to non-invasively estimate the LCORR wall thickness. In addition, the BRIS also provides vital information for the deduction of the DNA molecule density on the surface, as discussed later in Section 4. During the characterization, progressively higher concentrations of ethanol in water were injected into the LCORR, causing small increases in the fluid's RI. The WGM shifted to a longer wavelength in response to the RI increase in the core. A BRIS of 6.8 nm/RIU was then obtained by measuring the slope of the WGM shift versus the RI change. Figures for this derivation are presented in the supplementary material. This sensitivity corresponds to a wall thickness of approximately 4 μm, based on the theoretical model that we developed earlier (White et al., 2006a; Zhu et al., 2007b).

2.4. Surface activation

To begin the experiment, the HF-treated LCORR was rinsed with a 1:1 HCl:methanol mixture for 30 min, followed by the rinse with methanol. 3× SSC buffer, the running buffer for the entire experiment, was subsequently pumped through the LCORR at a volumetric flow rate of 15 μL/min for 10–15 min. This establishes the detection baseline for subsequent WGM spectral shift measurements. Then, 1% 3-APS in 3× SSC buffer was run through the LCORR for 30 min at 15 μL/min.

After this and each subsequent step, 3× SSC rinse was employed to remove the non-specifically bound molecules. Next, 10 μM of the 25-base DNA probe and 5 mg/mL DMA

were mixed in 3× SSC and pumped through for 1 h to crosslink aminated probes to the LCORR surface. Finally, the LCORR was filled with 3× SSC and ready for the detection of target DNA. After DNA detection, the LCORR could be regenerated by running low concentration of HF to etch off the deposited DNA and 3-APS molecules.

3. Experimental results

Because of the real-time data acquisition capabilities of the LCORR, each stage in the experiment may be monitored, from the amine-functionalization through target DNA hybridization. Fig. 2 plots the sensorgram for the surface activation described in the previous section and for the subsequent detection of a positive control target strand (25-base complementary DNA).

The total WGM shift at the beginning of each activation phase is caused additively by real and non-specific binding of reactant molecules to the LCORR surface and by small changes in the bulk RI of the core fluid due to dissolved materials. The non-specific binding and the bulk RI change can be removed by rinsing the LCORR with 3× SSC buffer, as indicated by the downward shift in the WGM spectral position. Consequently, the net WGM shift corresponds to predominant contribution from the actual binding and small portion of non-specific binding that could not be rinsed off. Based on Fig. 2, the net WGM shift for the 25-mer probe was 21 pm.

Fig. 3(A) explores the LCORR detection capability of distinguishing target DNAs of different strand lengths (25-mer, 50-mer, and 100-mer). The concentration of all DNA samples are 10 μM to ensure that the saturation WGM shift was reached. The WGM shifts were measured by comparing the post-rinse WGM position with the pre-target position, yielding a net shift value. Clearly, saturation signal values in Fig. 3(A) do not behave linearly with strand length. This is explainable by pointing out the increased likelihood of steric effects with longer nucleotide

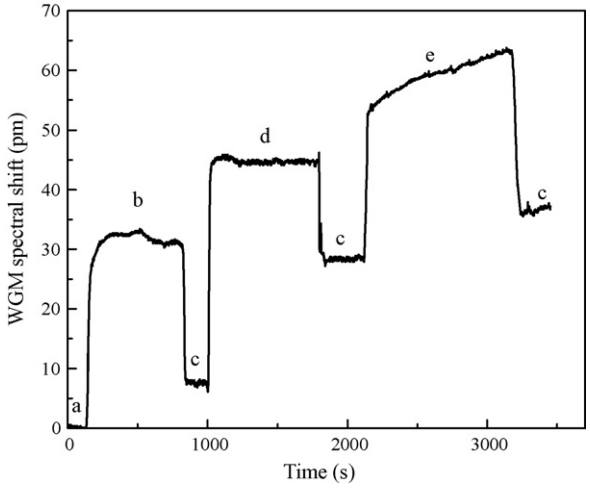

Fig. 2. Sensorgram for LCORR surface activation and 25-mer complementary target DNA detection. (a) initial baseline; (b) 3-APS modification; (c) buffer rinses with 3× SSC; (d) amine-modified probe DNA incubation; (e) target DNA incubation.

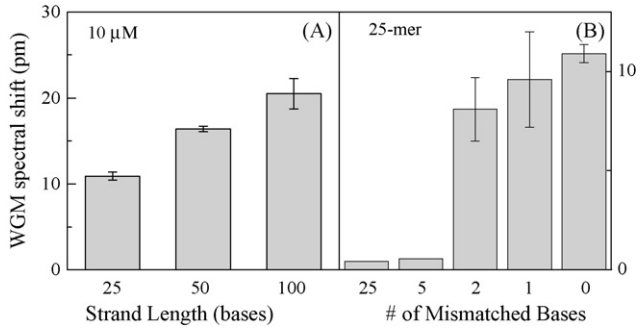

Fig. 3. Net WGM shift for various DNA strand lengths (A) and for various mismatches at the same 10 μM concentration (B). Hybridizations performed at 25 °C in 3× SSC buffer. Displayed standard deviations are 0.45, 0.32, and 1.77 pm for 25-mer, 50-mer, and 100-mer, respectively (A), and 1.6, 2.41, and 0.45 pm for 2-base, 1-base, and complimentary target (B).

chains. This effect is quantitatively investigated in Table 1 of the supplementary material.

Note that the quantitative comparisons in DNA strand length can only be achieved with this label-free detection. In fluorescence-based DNA microarray, the strand length information is lost and concentration estimation may be skewed due to the errors in fluorophore labeling. Fig. 3(B) investigates the LCORR's capability of detecting base-mismatched target DNA. In this experiment, various target DNA samples ranging from zero-base-mismatch (complementary DNA, positive control) to 25-base-mismatch (negative control) were used. All the DNA samples had the same strand length (25-base) and concentration (10 μM). With the increased mismatched bases, the net WGM shift drops gradually. For the single- and double-base mismatch targets, the difference in the net WGM shift is 1.3 and 2.8 pm, respectively. Although small, these differences are well within the system resolution capability (∼0.02 pm). Presently, the large standard deviation in this data makes repeatability a challenge, but subsequent work has already shown promise for improvement in this area. Given that the hybridizations were performed at room temperature, the conditions are far from optimized and there is reason to believe that this base-mismatch resolution could be improved. In fact, previous literature has demonstrated that buffer salt concentration can be adjusted to achieve as much as a 10 to 1 signal discrepancy between matched and single-base-mismatched strands (Vollmer et al., 2003). A significant decrease in the WGM net shift was observed when five or more bases are mismatched.

The results obtained in Fig. 3(B) can further be exploited in designing DNA assays to analyze the composition of mixed solutions of complementary and mismatched target strands, which has many important research and clinical applications such as DNA methylation studies in cancer patients (Jones and Laird, 1999; Fortina et al., 2002; Gitan et al., 2002). Fig. 3(B) indicates that the detection signal, *i.e.*, the net WGM shift, is small for 5-base-mismatch DNA, as compared to that for complementary DNA. Therefore, the LCORR should be able to clearly discriminate among mixed solutions of complementary and 5-base-mismatched target strands.

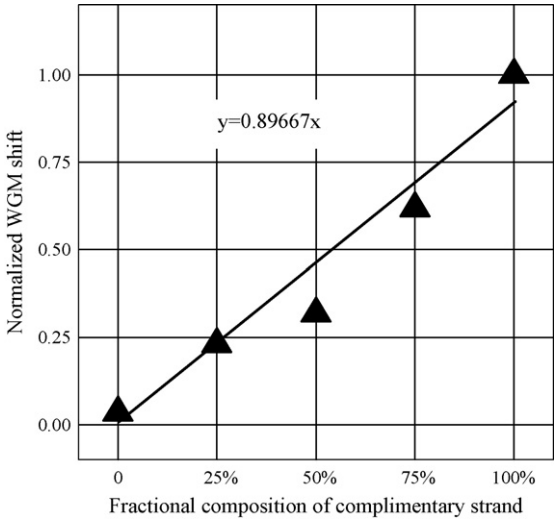

Fig. 4. Normalized net WGM shift as a function of the fractional composition of the complementary target DNA. DNA mixtures contain 25-mer complementary DNA and 5-base-mismatched 25-mer DNA. Total concentration: 10 μM.

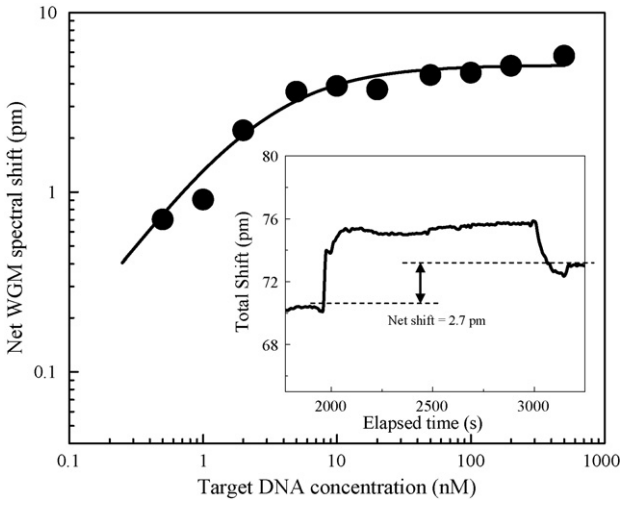

Fig. 6. Target DNA titration curve using 25-mer strands. Solid line: Michaelis–Menton curve fit using $K_d = 2.9$ nM and $\delta\lambda_{max} = 5.1$ pm. Insert shows net shift from 10 pM target using a 37 nm/RIU LCORR.

Fig. 4 shows good linearity ($R^2 = 0.946$) is obtained for various fractional compositions of the complementary strands. The regression line on this figure has a slope of 0.89667 (forced through the origin). Note that with zero complementary bases, we still see a small shift due to the contribution from the 5-base-mismatched DNA, as discussed earlier.

In addition to the net WGM shift, kinetic information can also be used to distinguish the base-mismatched DNA. Fig. 5(A) shows the binding curves for completely matched, 2-base-mismatched, 5-base-mismatched, and completely mismatched target 25-mer DNA strands. Although the final saturation WGM shift the three target DNA samples are close, their kinetic behavior is quite different. We can examine and model hybridization curves for DNA using a first-order Langmuir model for diffusion-limited interaction (Halperin et al., 2006):

$$\Gamma(t) = \Gamma_0[1 - \exp(-kt)], \tag{2}$$

where $\Gamma(t)$ is the sensor response signal as a function of time, t, and Γ_0 is the final signal plateau. k is the reaction rate constant (in units of s^{-1}) – which involves both hybridization and non-specific adsorption – and is plotted in Fig. 5(B) against the fraction of complementarity, which is defined as the fraction of DNA in the target strand that are complementary to the immobilized probe. Fig. 5(B) also shows an exponential fit to the rate constant, which demonstrates the high resolving power of kinetic analysis at low-mismatch (or high complementarity) values. This is very useful to reduce false positives when differentiating complementary DNA sample from those with only a few mismatched bases.

To evaluate concentration dynamic range of the LCORR DNA detection, we used complementary 25-base DNA ranging from 0.5 to 500 nM. The probes were immobilized on the LCORR interior surface as before, but the probe surface density was reduced in order to test the probe density effect on the LCORR sensing signal. The net WGM shift corresponding to the probe deposition was 12 pm, as compared to 21 pm obtained previously. Fig. 6 shows the net WGM shift in response to the target DNA concentration, which can be easily modeled as a function of bulk concentration using a form of Michaelis–Menton:

$$\delta\lambda_{WGM} = \frac{\delta\lambda_{max}[DNA]}{K_d + [DNA]}, \tag{3}$$

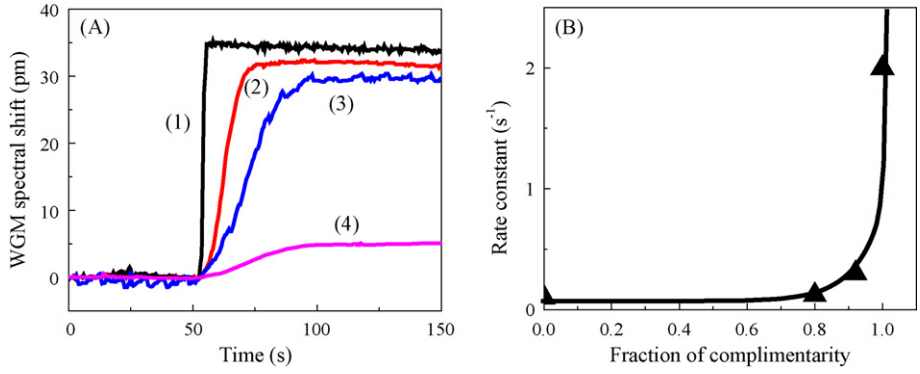

Fig. 5. (A) Kinetic data showing binding curves for DNA target that is (1) 100% complementary; (2) 2-base mismatch; (3) 5-base mismatch; (4) completely mismatch. (B) Triangles: rate constants extracted from (A) using a Langmurian model. Solid curve: exponential fit. DNA concentration: 10 μM.

where $\delta\lambda_{WGM}$ is the relative spectral shift, $\delta\lambda_{max}$ is the maximum possible shift observed for maximum surface coverage with target, K_d is the dissociation constant for hybridization, and [DNA] is the bulk concentration of the target strand. A Michaelis–Menton fit produces a dissociation constant K_d of 2.9 nM, close to what has been reported in previous studies (Lehr et al., 2003; Michel et al., 2007). $\delta\lambda_{max}$ is 5.1 pm, which is half of the saturation WGM shift when a higher probe density was used.

To further explore the detection limit of the LCORR, the inset of Fig. 6 is presented with a net shift for 10 pM 25-mer using an LCORR with much higher sensitivity (37.1 nm/RIU), achieved by wall thinning. This demonstrates that improved LOD is possible with further optimization.

4. Theoretical analysis

We have established a linear relationship between the WGM shift and the molecule density on the LCORR surface (Zhu et al., 2007a), which allows for detailed quantitative analysis of the molecule detection using the LCORR:

$$\delta\lambda = \sigma_p \alpha_{ex} \frac{2\pi\sqrt{n_2^2 - n_3^2}}{\varepsilon_0 \lambda} \frac{n_2}{n_3^2} S, \quad (4)$$

where $\delta\lambda$ is the WGM shift due to molecular deposition, σ_p is the molecular surface density in number of molecules per unit area, α_{ex} is the excess polarizability of the analyte, n_2 and n_3 are the RI of the LCORR capillary wall and the aqueous media in the core, respectively. ε_0 is vacuum permittivity, λ is the wavelength of the WGM, and S is the BRIS of the LCORR (in units of nm/RIU). In our experiment, $S = 6.8$ nm/RIU. n_3 is assumed to be equal to that of water, 1.33, and n_2 is 1.45 for silica. The excess polarizability for DNA scales linearly with molecular weight and has been determined to be $4\pi\varepsilon_0(4.4 \times 10^{-22}\ cm^3)$ for 25-mer DNA, $4\pi\varepsilon_0(8.9 \times 10^{-22}\ cm^3)$ for 50-mer DNA, and $4\pi\varepsilon_0(1.78 \times 10^{-21}\ cm^3)$ for 100-mer DNA (Nicolai et al., 1987; Vollmer et al., 2003).

Using Eq. (4) it is also possible to deduce the LOD for DNA molecules on the surface, since the WGM shift is linearly proportional to the molecule density of the surface. Assuming that 0.02 pm is our system resolution, which has been obtained in an earlier study (Zhu et al., 2007b), the LOD for molecule density can be estimated using the net WGM shift. Corresponding surface densities for each chemical activation stage are listed in the supplementary material. For 25-mer, 50-mer, and 100-mer DNA samples, the LOD's are 2.7×10^{10}, 1.5×10^{10}, and 6.8×10^9 molecules/cm^2, respectively. The molecular weights of those DNA samples are approximately 7.78, 16.01, and 31.57 kDa, for 25-mer, 50-mer, and 100-mer, respectively. Therefore, the LOD for mass loading can also be obtained.

According to our calculations the LOD for mass is on the order of 4 pg/mm^2 (in supplementary material), close to what is reported in label-free DNA detection based on microspheres (Vollmer et al., 2003) and SPR (Homola et al., 1999). The minimal detectable surface coverage was also calculated, where the maximal loading density is assumed to be 5.7×10^{13} molecules/cm^2. These values were 0.05%, 0.026%, and 0.012% for 25-mer, 50-mer, and 100-mer, respectively. Note that the minimal detectable surface coverage decreases progressively as the DNA strand lengths increases, since longer DNA carries larger mass.

5. Conclusions and future research

In this paper, we have developed a protocol for LCORR-based DNA assays. Detailed analysis of the LCORR response to a variety of DNA samples has been performed to evaluate the LCORR DNA detection capability. DNA molecules on the LCORR were quantified using the theoretical model that relates the sensing signal (WGM shift) to the molecule surface density. Bulk DNA detection of 10 pM 25-mer has been achieved and the actual limit of detection is significantly lower. The mass loading limit of detection is estimated to be 4 pg/mm^2, competitive with other label-free methods (Homola et al., 1999; Vollmer et al., 2003).

Further improvement in the LOD will be accomplished with a better BRIS by using a thinner wall. Polymers such as dextran, to which multiple DNA probes can be attached, will also be used to increase the mass loading on the surface (Vollmer et al., 2003). Furthermore, an additional reference channel can be used to reduce common-mode noise such as temperature fluctuation and non-specific binding. Non-specific binding can also be further reduced by using blocking agents. Currently, 40–50% hybridization has been achieved. In the future, temperature and buffer salt concentration will be optimized to obtain (Chao et al., 2006) higher hybridization. In the meantime, microfabricated waveguides in replacement of fragile-tapered optical fibers for DNA microarray development will also be investigated (White et al., 2006b).

Acknowledgements

The authors thank the support from the Wallace H. Coulter Foundation Early Career Award and 3M Non-Tenured Faculty Award.

Appendix A. Supplementary data

Supplementary data associated with this article can be found, in the online version, at doi:10.1016/j.bios.2007.10.005.

References

Araci, I.E., Mendes, S.B., Yurt, N., Honkanen, S., Peyghambarian, N., 2007. Opt. Express 15 (9), 5595–5603.
Chao, C.-Y., Fung, W., Guo, L.J., 2006. IEEE J. Selected Topics Quantum Electron. 12 (1), 134–142.
Charles, P.T., Vora, G.J., Andreadis, J.D., Fortney, A.J., Meador, C.E., Dulcey, C.S., Stenger, D.A., 2003. Langmuir 19 (5), 1586–1591.
Chinowsky, T.M., Quinn, J.G., Bartholomew, D.U., Kaiser, R., Elkind, J.L., 2003. Sens. Actuator B: Chem. 91 (1–3), 266–274.
Christopoulos, T.K., 1999. Anal. Chem. 71 (18), 425R–438R.
Cox, W.G., Singer, V.L., 2004. Biotechniques 36 (1), 114–122.
Fan, X., White, I.M., Zhu, H., Suter, J.D., Oveys, H., 2007. SPIE Laser Resonators Beam Control X 6452, 64520M.

Fortina, P., Surrey, S., Kricka, L.J., 2002. Trends Mol. Med. 8 (6), 264–266.
Gill, P., Jeffreys, A.J., Werrett, D.J., 1985. Nature 318 (6046), 577–579.
Gitan, R.S., Shi, J., Chen, C.-M., Yan, P.S., Huang, T.H-M., 2002. Genome. Res. 12 (1), 158–164.
Golden, J.P., Anderson, G.P., Rabbany, S.Y., Ligler, F.S., 1994. IEEE Trans. Biomed. Eng. 41 (6), 585–591.
Gorodetsky, M.L., Ilchenko, V.S., 1999. J. Opt. Soc. Am. B 16 (1), 147–154.
Gorodetsky, M.L., Savchenkov, A.A., Ilchenko, V.S., 1996. Opt. Lett. 21 (7), 453–455.
Guo, Z., Guilfoyle, R.A., Thiel, A.J., Wang, R., Smith, L.M., 1994. Nucleic Acids Res. 22 (24), 5456–5465.
Halperin, A., Buhot, A., Zhulina, E.B., 2006. J. Phys. Condens. Matter 18 (18), S463–S490.
Homola, J., Yee, S.S., Gauglitz, G., 1999. Sens. Actuator B: Chem. 54 (1–2), 3–15.
Jones, P.A., Laird, P.W., 1999. Nat. Genet. 21 (2), 163–167.
Lehr, H.-P., Reimann, M., Brandenburg, A., Sulz, G., Klapproth, H., 2003. Anal. Chem. 75 (10), 2414–2420.
Lin, H., Musick, M.D., Nicewarner, S.R., Salinas, F.G., Benkovic, S.J., Natan, M.J., Keating, C.D., 2000. J. Am. Chem. Soc. 122 (36), 9071–9077.
Lin, B., Qiu, J., Gerstenmeier, J., Li, P., Pien, H., Pepper, J., Cunningham, B., 2002. Biosens. Bioelectron. 17 (9), 827–834.
Luong, J.H., Bouvrett, P., Male, K.B., 1997. Trends Biotechnol. 15 (9), 369–377.
Michel, W., Mai, T., Naiser, T., Ott, A., 2007. Biophys. J. 92 (3), 999–1004.
Nicolai, T., Van Dijk, L., Van Dijk, J.A.P.P., Smit, J.A.M., 1987. J. Chromatogr. 389, 286–292.
Passaro, V.M.N., Dell'Olio, F., Casamassima, B., De Leonardis, F., 2007. Sensors 7 (4), 508–536.
Ramachandran, N., Larson, D.N., Stark, P.R.H., Hainsworth, E., LaBaer, J., 2005. FEBS J. 272 (21), 5412–5425.
Schneider, B.H., Dickinson, E.L., Vach, M.D., Hoijer, J.V., Howard, L.V., 2000. Biosens. Bioelectron. 15 (1–2), 13–22.
Sepulveda, B., Sanchez del Rio, J., Moreno, M., Blanco, F.J., Mayora, K., Dominguez, C., Lechuga, L.M., 2006. J. Opt. A: Pure Appl. Opt. 8 (9), S561–S566.
Vollmer, F., Braun, D., Libchaber, A., Khoshsima, M., Teraoka, I., Arnold, S., 2002. Appl. Phys. Lett. 80 (21), 4057–4059.
Vollmer, F., Arnold, S., Braun, D., Teraoka, I., Libchaber, A., 2003. Biophys. J. 85 (3), 1974–1979.
White, I.M., Oveys, H., Fan, X., 2006a. Opt. Lett. 31 (9), 1319–1321.
White, I.M., Oveys, H., Fan, X., Smith, T.L., Zhang, J., 2006b. Appl. Phys. Lett. 89 (19), 191106.
White, I.M., Zhu, H., Suter, J.D., Hanumegowda, N.M., Oveys, H., Zourob, M., Fan, X., 2007. IEEE Sens. J. 7 (1), 28–35.
Ymeti, A., Greve, J., Lambeck, P.V., Wink, T., van Hovell, S.W.F.M., Beumer, T.A.M., Wijn, R.R., Heideman, R.G., Subramaniam, V., Kanger, J.S., 2007. Nano Lett. 7 (2), 394–397.
Zhu, H., White, I.M., Suter, J.D., Dale, P.S., Fan, X., 2007a. Opt. Express. 15 (15), 9139–9146.
Zhu, H., White, I.M., Suter, J.D., Zourob, M., Fan, X., 2007b. Anal. Chem. 79 (3), 930–937.
Zuker, M., 2003. Nucleic Acids Res. 31 (13), 3406–3415.